Verification of wind tunnel model support and wall interference assessments in DNW-HST by CFD simulations

Frenk Wubben
German-Dutch Wind Tunnels DNW
P.O. Box 175, 8300 AD Emmeloord
THE NETHERLANDS

Frenk.wubben@dnw.aero

Hans Maseland
Netherlands Aerospace Centre NLR
P.O. Box 90502, 1006 BM Amsterdam
THE NETHERLANDS

Hans.maseland@nlr.nl

ABSTRACT

The DNW-HST is a closed-circuit, pressurized transonic wind tunnel facility that has a test section with slotted upper and lower walls. As part of a continuous effort to reduce the uncertainty of 'free-flow' test results from this tunnel, activities have been undertaken to verify the adequacy of the correction methods for model support and wall interference effects. In this paper a RANS-based Computational Fluid Dynamics (CFD) method is utilized to generate data for a test article in a free flow as well as in a wind tunnel environment that closely resembles the DNW-HST, including a nozzle, test section with slotted walls, plenum chamber, flow re-entry area and diffusor. In this numerical wind tunnel, empty test section flow calibrations, support interference and wall interference assessments have been performed according to the commonly adopted experimental procedures. The CFD results for the test article in the wind tunnel environment are then corrected according to the experimental procedures, and are compared to the numerical simulation in free flow conditions. Final residues for lift and drag appear to be in the order of experimental uncertainty levels.

1.0 INTRODUCTION

As part of a continuous effort to reduce the uncertainty of 'free flow' test results at the High-Speed Tunnel (HST) of the German-Dutch Wind Tunnels (DNW), multiple validation and verification activities have been undertaken to assess the adequacy of the correction procedures for wind tunnel interference effects like support and wall interference. The following activities were recently performed:

1. Tunnel-to–Tunnel comparison: using corrected experimental results from DNW-HST and ETW (ref. [1]).
2. Tunnel-to-CFD comparison: using corrected experimental results and numerical simulation results for free flow conditions (ref. [1]).
3. Comparisons of corrected experimental results obtained on two different model support systems in DNW-HST (ref. [2]).
4. CFD-to-CFD comparison: using corrected results obtained in a numerical wind tunnel, versus numerical simulation results for free-flow conditions.

The aim of this last activity is to verify the experimental bookkeeping procedures by using CFD. To this end, CFD simulations are conducted for the test article in the wind tunnel environment, as well as simulations in the free flow environment at identical reference flow conditions (see figure 1-1).

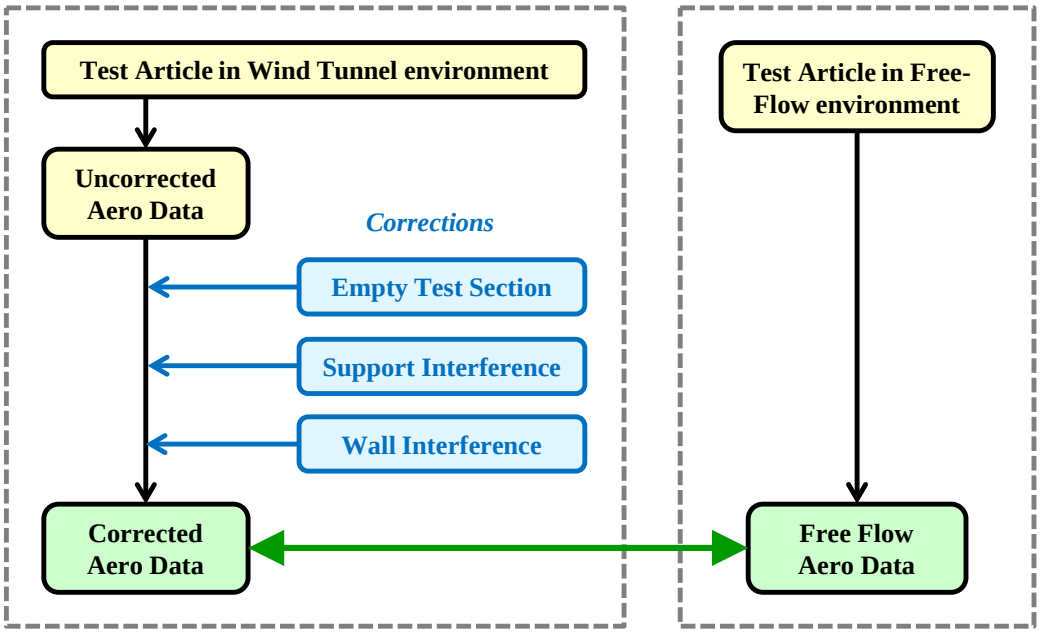

Figure 1-1: Verification scheme

In the **wind tunnel environment**, the CFD simulation results provide aerodynamic data of the test article with all tunnel interferences included. Specific simulations are performed in alternative test setups to discriminate the constituent components, i.e. empty test section flow, model support and wall interference effects. After correction for these interference effects, 'fully corrected' aerodynamic data are obtained that can be directly compared with **free flow aerodynamic data**.

The benefit of using CFD is that it offers the possibility to provide consistent results for both environments which is not possible in an experimental approach. Furthermore, systematic CFD errors are circumvented where in this study only differences between CFD results are assessed.
Hereby, this study should lead to a better understanding where differences occur and potentially where improvements in the experimental bookkeeping approach are necessary. Because the purpose is to verify the bookkeeping procedure, it should be noted that it is not necessary to have an exact representation of the DNW-HST. The bookkeeping should work for comparable wind tunnels as well. Nevertheless, it is aimed for to have sufficient detailing in the CFD simulations to achieve a wind tunnel that closely resembles the real DNW-HST. The numerical wind tunnel interference results are compared with experimental results to validate the representativeness of the corrections.

2.0 WIND TUNNEL FACILITY AND TEST ARTICLE

The DNW-HST situated in Amsterdam is a closed-circuit, variable pressure transonic wind tunnel facility used by industry to support the development of new aircraft and launch vehicles at high Reynolds numbers (see figure 2-1). An adjustable nozzle is followed by a rectangular test section with solid side walls and movable slotted upper and lower walls with openness ratio of 12%. The upper and lower walls can be adjusted to obtain a test section height of 1.60 m or 1.80 m. The width of the test section is 2.0 m. The test section is surrounded by a plenum chamber to accommodate in- and outflow from the test section. The stagnation pressure can be varied between 20 and 390 kPa. The tunnel is calibrated for Mach numbers between 0.20 and 1.30. The test section contains a permanently installed vertical strut with the so-called boom-base adapter which allows for mounting of various types of model support systems. The upper, lower and sidewalls of the test section are equipped with multiple rows of pressure taps.

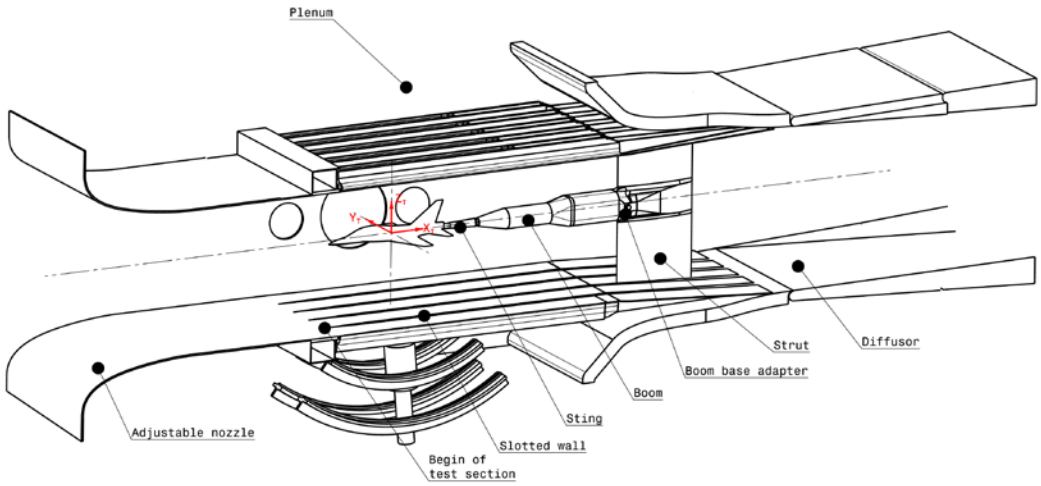

Figure 2-1: Schematic view of DNW-HST nozzle, test section and diffusor

The test article is a 1:15 full-span scaled version of a business jet, with rear fuselage mounted through flow nacelles, wing span of 1.28 m and wing mean aerodynamic chord of 0.171 m. The cruise Mach number is 0.78. The test article was used for measurements in DNW-HST in 2014 (see ref [1]). The same test article is used for the investigations reported in this paper. A wing-body-pylon-nacelle configuration is used for the current study.

3.0 EXPERIMENTAL BOOKKEEPING PROCEDURE

3.1 Sources of interference

A well-known feature of wind tunnel testing is that the presence of test section walls and the commonly required model support system impose systematic uncertainties to the actual test conditions and related measurement results. In the bookkeeping procedure of DNW-HST, the following main sources of systematic uncertainties are postulated (see figure 3-1):

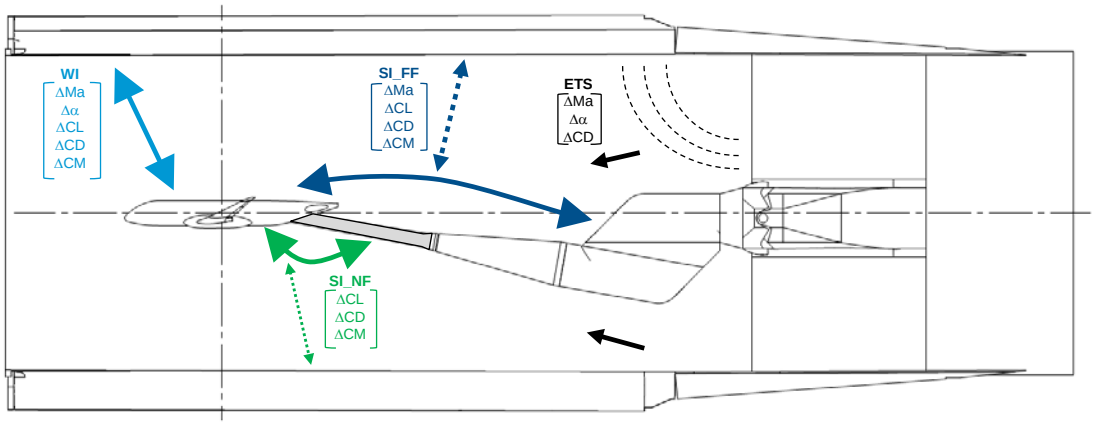

Figure 3-1: Overview of wind tunnel interference effects

1. **Empty test section (ETS) interference effect** which is defined as the flow non-uniformity in angle of attack, Mach number and axial pressure gradient due to the sustained channel flow of the empty wind tunnel including the vertical strut and boom base adapter. The latter represents non-removable parts of the tunnel configuration. In the empty test section, the test article and movable support systems are absent.
2. **Support interference (SI) effects** can be split in near field (SI_NF) and far field (SI_FF) contributions (see ref. [3]). Far field effects are corresponding to the entire flow field disturbance due to the presence of the support boom in the test section. Near field effects are originating from the direct (local) interaction of the sting with the test article. An open cavity will be present in the test article to facilitate the passage of the sting. Due to this cavity, a resultant force and moment is present which is implicitly part of the model support correction. It should be noted that the support system also has an interaction with the wind tunnel walls (dashed arrows in figure 3-1). In the bookkeeping procedure, all these effects are contributed to support interference corrections.
3. **Wall interference (WI) effects** arise from the interaction of the test article flow with the test section walls.

3.2 Empty test section interference

Empty test section interference effects are measured along the centreline of the wind tunnel by means of a long tube equipped with static pressure taps (referred to as the long static tube). The static pressure at the tunnel centreline is measured in reference to the static pressure in the plenum chamber (p_{pl}) and hence establishes a calibration for a range of Mach numbers. This calibration (see figure 3-2) is subsequently employed to set the reference Mach number (Ma_{ref}) at the Model Reference Point (MRP). The calibrated centerline pressure distribution also serves to calculate the drag increment that the test article experiences due to the buoyancy effect of the test section. During the long static tube calibration measurements, the boom base adapter on the vertical strut is positioned on the tunnel centreline.

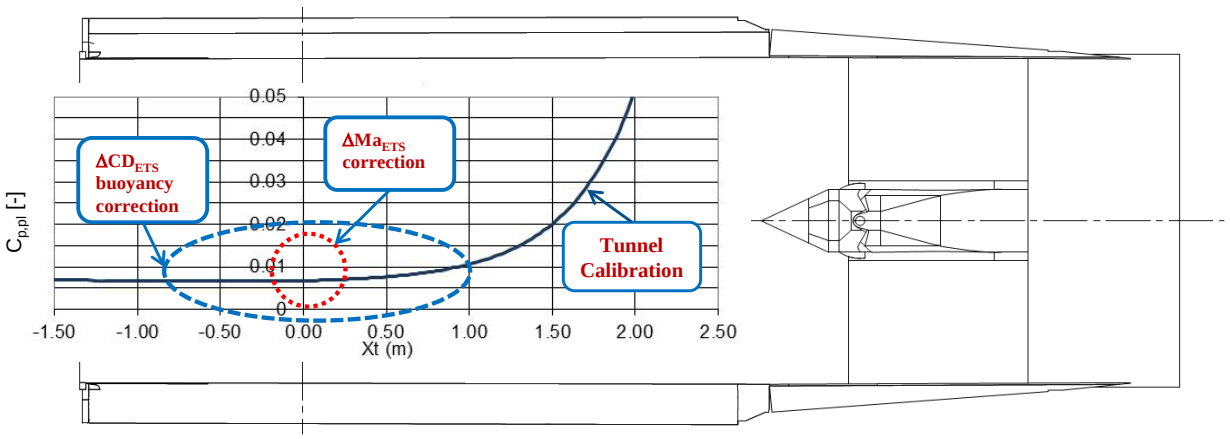

Figure 3-2: Illustration of empty test section geometry and calibrated pressure distribution.

In the bookkeeping procedure it is assumed that the flow non-uniformities in the empty test section have a negligible impact on lift and pitching moment. The mean flow angularity is determined from measurements with the test article and support system oriented at a baseline and inverted position. Flow upwash angles are derived from the differences between lift versus alpha curves for both the baseline and inverted orientations.

3.3 Support interference

Due to the presence of the model support system, flow distortions are present that change the static pressure distribution in the empty test section and consequently, the reference Mach number at the MRP. For this reason, a dedicated long static tube calibration is performed with the support boom mounted in the test section (see figure 3-3). Ideally, the sting should be included as well, but this part of the support system physically interferes with the long static tube. The effect of the sting is assumed to be small and therefore neglected. Hence this calibration is considered as a far and near field calibration and is used for setting the reference Mach number during the test with the actual test article and support system present.

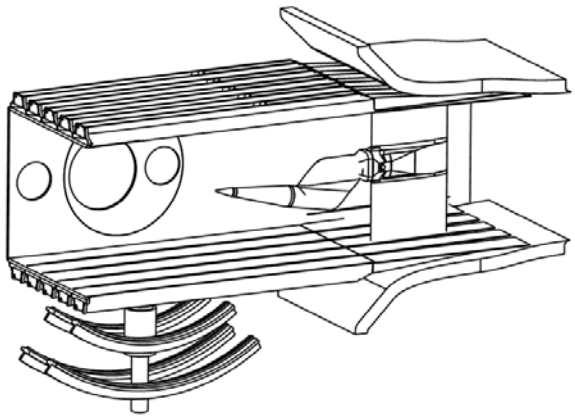

Figure 3-3: Test section with support boom (ETS + DRB)

Combined far and near field support interference for a test article can be measured in the tunnel environment using a multiple support arrangement. To this end, a floor mounted dorsal system is introduced to support the inverted test article (see figure 3-4). The original rear support is employed as a dummy support. Aerodynamic forces and moment coefficients are measured with an internal balance. During the measurements, there is no contact between the dummy rear support and the test article. Great care is taken to ensure that the test article and dummy rear support are aligned likewise as during the rear support measurements. Model support corrections are derived from balance measurements with and without the presence of the dummy rear support.

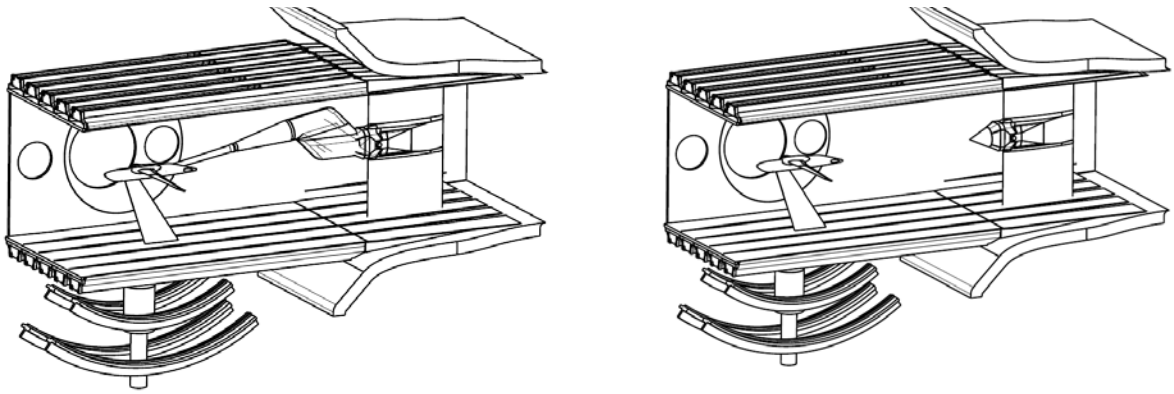

Figure 3-4: Support interference configurations; Left picture: dummy rear support present; Right picture: dummy rear support removed

Corrections for lift, drag and pitching moment coefficients are obtained from the difference in results between the setups with and without dummy rear support, both acquired at identical reference Mach number and angle of attack. For the configuration **with** dummy rear support, the Mach number calibration for rear model support boom is applied. For the configuration **without** dummy rear support boom, the Mach number calibration of the empty test section is applied. This ensures the same reference Mach number at the MRP for both test setups. Both test article setups experience different local flow non-uniformities which are manifested as differences in the aerodynamic coefficients. The dorsal support will interfere as well with the flow in the vicinity of the test article, but it is assumed that the effect of the dorsal support is the same in both setups and cancels out after subtraction of the results from both setups.

3.4 Wall interference

A measured wall pressure signature method is used for assessment of wall interference effects. The method is called WIN3VE (acronym for: Wall Interference, 3D test article, Ventilated test section) and was developed by NLR (ref. [4]). The method is based on linearized potential flow theory, with a Prandtl-Glauert compressibility correction. In essence, WIN3VE is built on the assumption that the walls are far enough away from the test article, such that their interaction can be modelled as a linear perturbation of the empty test section flow field. The measured pressures at the walls are affected by flow disturbances from the empty test section, model support, test article and interaction effects of the test article with the walls. Wall effects of the empty test section and model support are already included in the empty test section and support interference calibration correction. Hence, these effects are removed by subtraction of the wall pressures for the isolated support boom (see figure 3-5). This also has the advantage that smooth wall pressure distributions are obtained.

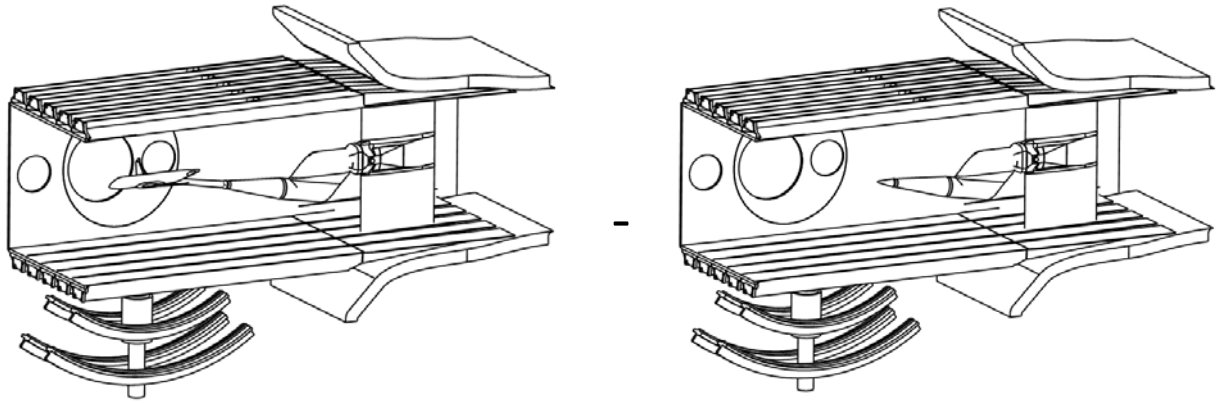

Figure 3-5: Configurations used for taring wall pressure data. Left: test article and rear support. Right: setup with isolated double roll boom.

In the current bookkeeping approach, DNW only corrects wall interference effects by a wall-induced buoyancy correction on drag. Corrections for angle of attack and blockage are relatively small, therefore difficult to verify and hence, not standard applied yet.

3.5 Overview of applied interference attributions

Equation (1) summarizes the interference attributions that are accounted for in the experimental bookkeeping. The results with the subscripts ‘COR’ and “UNC” correspond to corrected and uncorrected measurement data respectively. As presented in equation (1), corrections are applied to the Mach number (Ma), associated flow quantities, such as static pressure, dynamic pressure and Reynolds number, angle of attack (α), lift coefficient (CL), drag coefficient (CD) and pitching moment coefficient (CM).

$$\begin{Bmatrix} Ma \\ \alpha \\ CL \\ CD \\ CM \end{Bmatrix}_{COR} = \begin{Bmatrix} Ma \\ \alpha \\ CL \\ CD \\ CM \end{Bmatrix}_{UNC} + \begin{Bmatrix} \Delta Ma \\ \Delta\alpha \\ - \\ \Delta CD \\ - \end{Bmatrix}_{ETS} + \begin{Bmatrix} \Delta Ma \\ - \\ \Delta CL \\ \Delta CD \\ \Delta CM \end{Bmatrix}_{SI\_FF} + \begin{Bmatrix} - \\ - \\ \Delta CL \\ \Delta CD \\ \Delta CM \end{Bmatrix}_{SI\_NF} + \begin{Bmatrix} - \\ - \\ - \\ \Delta CD \\ - \end{Bmatrix}_{WI} \quad (1)$$

4.0 NUMERICAL APPROACH

4.1 General

As basis for the verification approach, a CFD method is used to generate aerodynamic data for the test article in **free flow** condition as well as in a **wind tunnel environment.** Numerical investigations are performed for cruise Mach number 0.78, angle of attack 2.5° and Reynolds number of 3 million, based on the mean aerodynamic chord. In this paper, results are only presented for this flow condition. Flow conditions at Mach numbers 0.50 and 0.83 are investigated as well but results are not available yet for presenting in this paper.

Only a selected part of the wind tunnel circuit is simulated and the CFD representation therefore features artificial inflow and outflow planes. The exit plane is located in the diffuser. At the entry side a straight elongation of the test section entrance has been assumed (no contraction). A set of boundary conditions is specified at these artificial inflow/outflow planes in order to set the flow in the tunnel duct. This is accomplished by means of the total pressure at the inflow plane and a static pressure at the outflow plane. The reference flow conditions are defined at the MRP and are given by the Mach number, Ma_{ref}, and Reynolds number, Re_{ref}. The simulations are based on the RANS equations in combination with a two-equation k-ω turbulence model to account for the turbulent stresses. Here, the Explicit Algebraic Reynolds Stress Model (EARSM) formulation is used (see ref. [5] and [6]). The RANS equation is solved using an iterative procedure to ensure balance of the energy, momentum and mass fluxes. Integrating the mass flux on the inlet and outlet boundary still give a small numerical leak, typically about 0.1% of the incoming mass flux. This numerical leak can be attributed to amongst others numerical dissipation implied by discretization of the RANS equation.

At the start of a simulation, the flow variables are initialised using stagnant values. The flow in the tunnel representation develops by performing 20000 single grid iterations on the medium grid level. Subsequently, 10000 multi-grid cycles are performed on the fine grid level to capture the viscous flow phenomena associated to boundary layers and wakes. In case, the tunnel flow solutions features unsteady flow phenomena, an averaging procedure was employed. The CFD results in this paper are limited to lift and drag coefficients.

4.2 Computational procedure for calibrations

The following two configurations are considered for the test section calibrations:

1. Empty test section (ETS)
2. Empty test section and double roll boom support system (ETS+DRB). The position and orientation of the double roll boom are determined by the kinematics that corresponds to the incidence angle of the test article.

The present numerical work adopts the outlined experimental procedure for setting the flow in the test section. The objective for setting the Mach number to a value of M_{ref} at the MRP, at Reynolds number, Re_{ref}, is translated into the condition for the static pressure coefficient:

$$C_p = \frac{P - P_{ref}}{Q_{ref}} = 0 \qquad (2)$$

where the reference values are evaluated at the MRP. The desired Mach number is obtained in an iterative way from flow simulations for specific pressure values at the outflow plane (also referred to as the exit pressure). In practice, two solutions provide the starting values and linear interpolation or extrapolation is utilized to arrive at the desired value. Note that at least 3 flow simulations are required for each configuration to arrive at the target flow condition. This work procedure is illustrated in figure 4-1 which depicts the Cp value at the MRP versus the exit pressure at the outflow boundary. Figure 4-1 shows that the presence of the DRB has a distinctive influence on the test section flow which translates into a particular setting of the exit pressure for a given Mach number at the MRP.

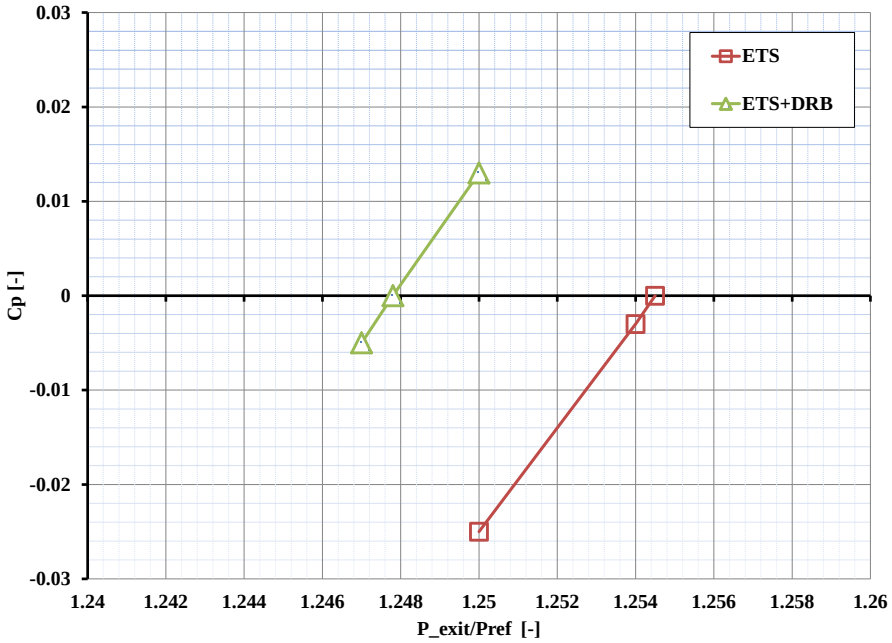

Figure 4-1: Mach number setting at MRP by variation of exit pressure ratio (P_{exit}/P_{ref});

For each Mach number, the corresponding plenum pressure coefficient is determined and is subsequently employed for setting the Mach number in simulations with test article present in the test section.

4.3 Computational strategy for simulations of test article setups

An overview of the considered test article setups in this study are provided in table 4-1. In addition, the selected tunnel calibration for the reference Mach number is given.

The computational grids for the test article setups are based on a unified block decomposition of the flow domain and feature identical grid point distributions in large parts of the computational domain. In order to reduce the flow calculation effort by a factor of two, the geometrical symmetry property of the full span test article and test section are employed to construct a computational mesh for the port-side half of the tunnel only. The computational grid for the port-side half of the tunnel consists of 47 million grid points. The numerical tunnel calibration data that has been established in the previous section is now utilised to set the reference flow for the configurations including the test article. The value of the static pressure coefficient in the plenum now becomes the target value that has to be met. The linear regression approach

is again employed to arrive at the target value. Figure 4-2 provides pressure coefficient distribution in the tunnel symmetry plane (y=0) for the dorsal set-up configurations with and without the dummy double roll boom support.

Table 4-1: Considered test article setups and corresponding tunnel calibration.

Configuration	Tunnel Calibration
1. **Free flying test article in tunnel (Model + ETS)**	**ETS**
2. **Test article on double roll boom support (Model + DRB + ETS)**	**ETS+DRB**
3. **Test article on dorsal support (Model + Dorsal + ETS)**	**ETS**
4. **Test article on dorsal support plus dummy double roll boom support (Model + Dorsal + DRB + ETS)**	**ETS+DRB**

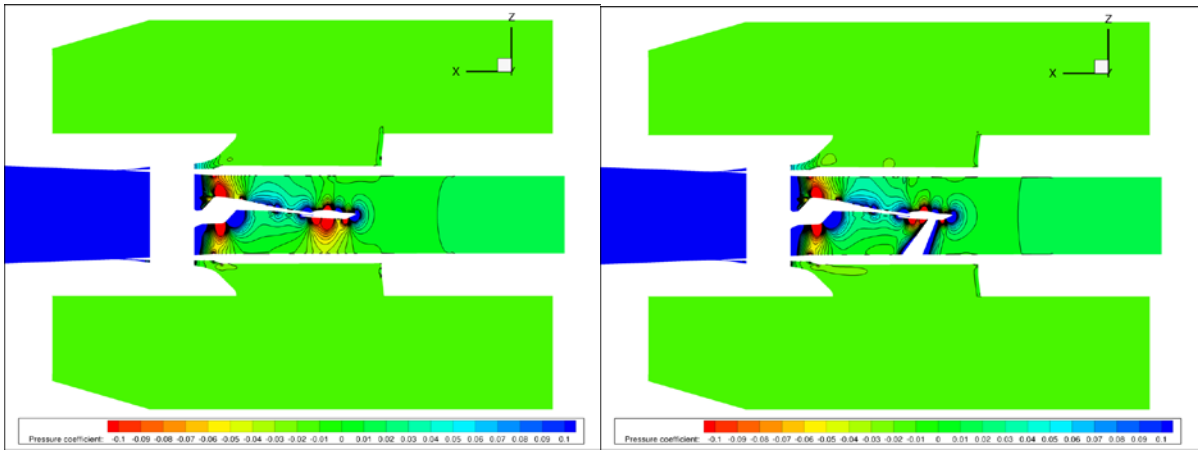

Figure 4-2: Cp distribution slice; Left: Model+DRB+ETS configuration; Right: Model+Dorsal+DRB+ETS

5.0 RESULTS

5.1 Empty test section

Figure 5-1 presents the numerical centreline pressure distribution in comparison to the experimental results for the empty test section (ETS). The pressure coefficient results are presented in reference to the plenum pressure of the respective wind tunnel (either the CFD wind tunnel or the experimental wind tunnel). For the reference Mach number shown, the numerical solution provides a different value for the plenum pressure compared to the experimental results. The differences in $C_{P,pl}$ between the experimental and numerical results are within 0.004. The figure shows that in the region where the test article is expected, a negative pressure gradient is present which leads to a buoyancy effect of 0.0001 in drag coefficient for the test article.

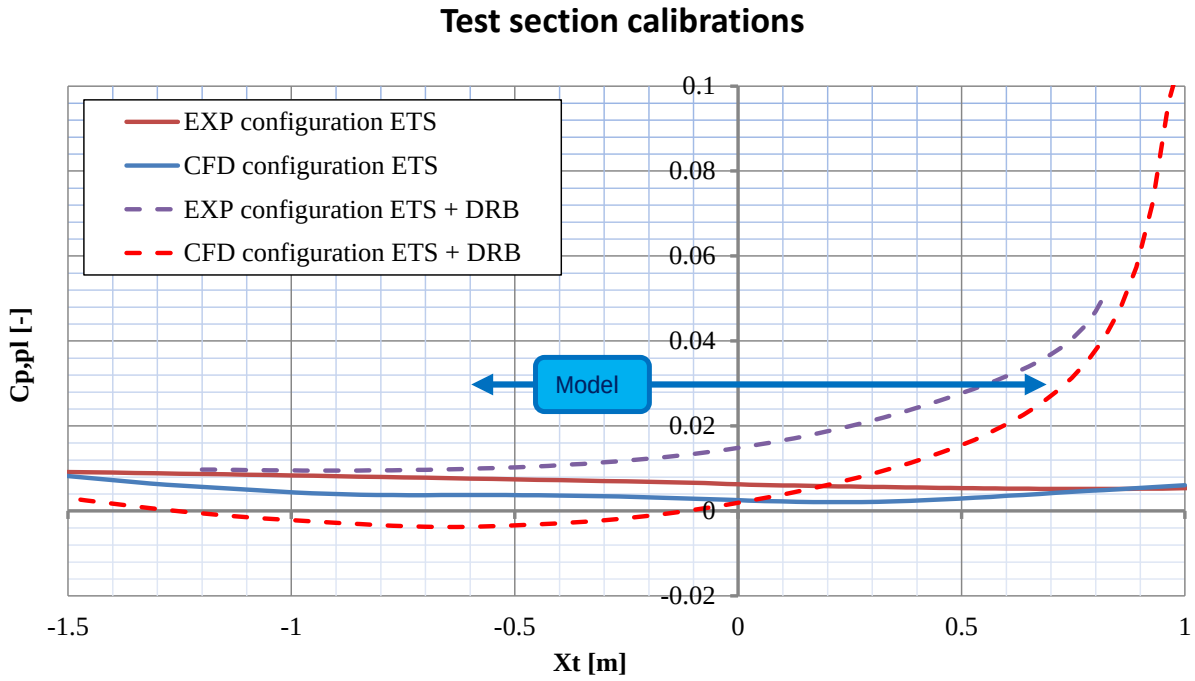

Figure 5-1: Experimental (EXP) and numerical (CFD) test section calibrations for the ETS configuration and ETS + DRB configuration; Ma = 0.78

5.2 Support interference effects

5.2.1 Flow condition

Figure 5-1 also provides the numerical and experimental test section pressure distribution for the ETS+DRB configuration. Although the trends in the pressure distribution for both wind tunnels are the same, differences in the order of 0.01 appear between the numerical and experimental pressure coefficients. For the same reference static pressure in the test section (i.e. the same reference Mach number), a difference in plenum pressure is present between the numerical and experimental results. This is an indication that the numerical wind tunnel behaves somewhat different than the experimental wind tunnel, which is thought of to be due to differences in the slot and re-entry flow between the two wind tunnels. This is the very reason why dedicated test section calibrations were made for each wind tunnel to ensure that results could be compared at the same reference Mach number.

5.2.2 Integrated forces and moments

The computation of aerodynamic forces and moment coefficients is carried-out by integrating the pressure and skin friction distributions over the surface of the test article. The surface area of the test article is slightly different for each configuration (see figure 5-4) due to the presence of cavities introduced to the fuselage to facilitate the stings. It is assumed that the effect of the dorsal cavity will cancel out after subtraction of results from configurations with a dorsal cavity. The surface area discrepancy related to the cavity for the (dummy-) rear sting of the double roll boom support is accounted for in the drag evaluation by means of a surface area ratio correction.

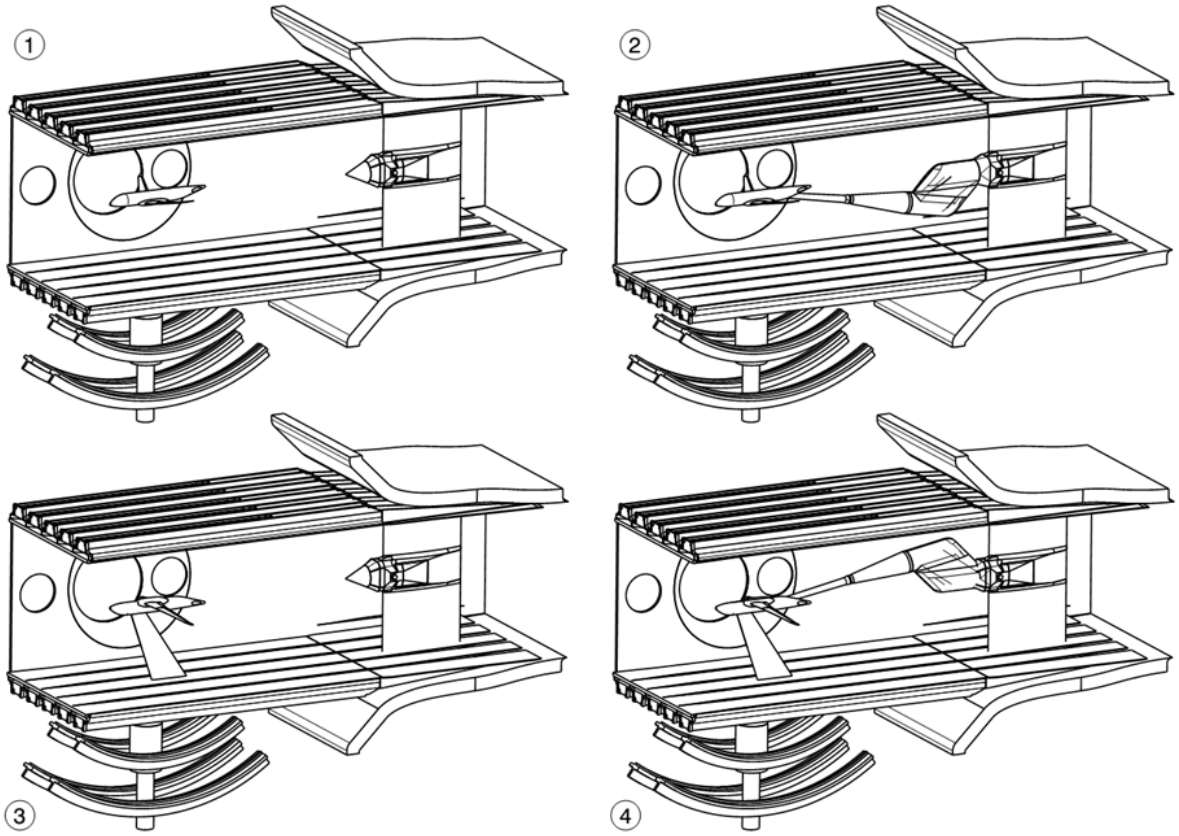

Figure 5-4: Definition of support interference configurations; Determination of support interference effects

Using the four configurations shown in figure 5-4, it is possible to determine the interference of the DRB support in two ways. First, the support effects are derived from the difference between configurations 1 and 2 (referred to as set 1); second as the difference between configurations 3 and 4 (referred to as set 2). This permits a consistency check on the predicted support interference increments and provides an indication of any mutual interference between the dorsal support and the dummy rear support. Table 5-1 shows results for the condition Ma=0.78 and alpha=2.5°.

Table 5-1: Support interference increments from different configurations for Ma=0.78 and alpha=2.5°

SI set (configurations) : source	ΔCL [-]	ΔCD [-]
Set 1 (1-2): via **CFD** data	-0.0220	0.0034
Set 2 (3-4): via **CFD** data	-0.0162	0.0036
Set 2 (3-4): via **Experimental** data	-0.0135	0.0039

The increments in lift and drag coefficient are presented for sets 1 and 2 (as based on CFD), along with the increment found in the real wind tunnel experiment. A comparison of the CFD increments of set 1 and 2 shows differences for lift coefficient of 0.006 and 0.0002 for drag coefficient. The differences might be an indication for mutual interference between the dorsal and rear support but might also result from

uncertainties in the CFD approach. The differences between set 2 and the experiment are 0.003 for lift and 0.0003 for drag.

5.3 Wall interference effects

Wall interference effects are determined in two ways. First, direct wall interference effects are determined from test article simulations in the empty test section and in free flow (see figure 5-5). These data are referred to as set A. The flow solution in the wind tunnel is affected by the test article, wall interference and empty test section effects. In order to obtain only wall interference effects, the tunnel simulation results are subtracted by the free flow results and subsequent correction for empty test section effects by a buoyancy correction on drag.

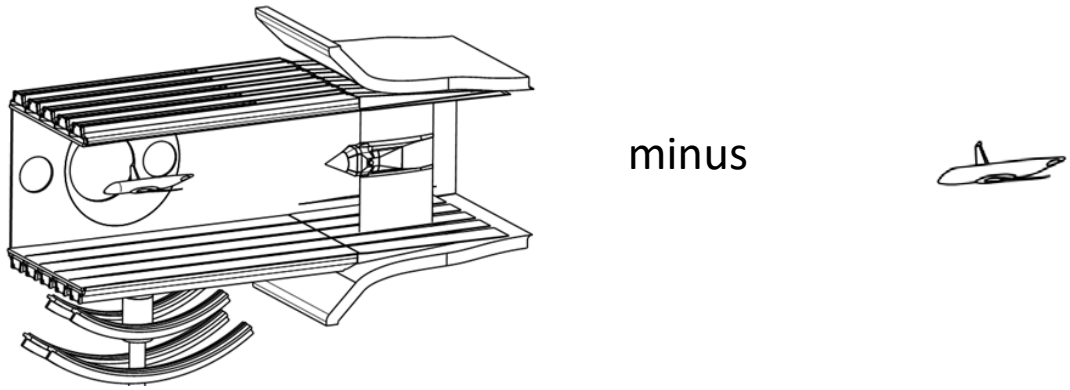

Figure 5-5: Determination of wall interference effects using results obtained for a wind tunnel environment and free flow

Second, wall interference results are determined from the WIN3VE wall pressure signature method using tared wall pressures from the configurations earlier presented in figure 3-5. This is performed by using numerical results as well as experimental results (set B). Table 5-2 gives a comparison of the results of sets A and B.

Table 5-2: Wall interference (WI) increments for Ma=0.78 and alpha=2.5°

WI set : source (configurations)	ΔCL [-]	ΔCD [-]	ΔMa [-]	Δα [°]
Set A: *direct*, via CFD data	**0.0015**	**0.0011**	**-**	**-**
Set B: WIN3VE based on CFD data	**0**	**0.0013**	**0.0037**	**0.005**
Set B: WIN3VE based on Experimental data	**0**	**0.0006**	**-0.0001**	**-0.048**

It appears that wall interference effects are more severe in the numerical wind tunnel (ΔCD=0.0013) compared to the experimental wind tunnel (ΔCD=0.0006). This is also illustrated in figure 5-6, where tared wall pressure distributions from CFD and experiment are presented as function of test section axial coordinate X_t. The taring is performed with the ETS + DRB wall pressure distributions from the respective wind tunnel (see figure 3-5). The tared data still contains a footprint of the pressure field of the test article. In a next processing step, this test article-induced pressure field is subtracted (see paragraph 3-3). The figure shows differences in the closed part of the test section (X_t < -1.225 m). The numerical tunnel shows

ΔC_p levels which are almost zero at X_t = -2.5 m, rising up to levels of about 0.006 at the start of the slotted test section (X_t = -1.225 m), whereas the experimental results shows an elevated pressure level of about 0.01 in ΔC_p in the closed part of the test section. Downstream of the test article, differences between the numerical and experimental wind tunnel are noticeable as well. The observed pressure differences can be explained from a difference in flow volumes leaving the test section to the plenum chamber. This mechanism is affected by the pressure difference over the wall slots and the wind tunnel re-entry area. From experiments, it is known that the flow field in the test section is influenced by variations of the re-entry cross section area.

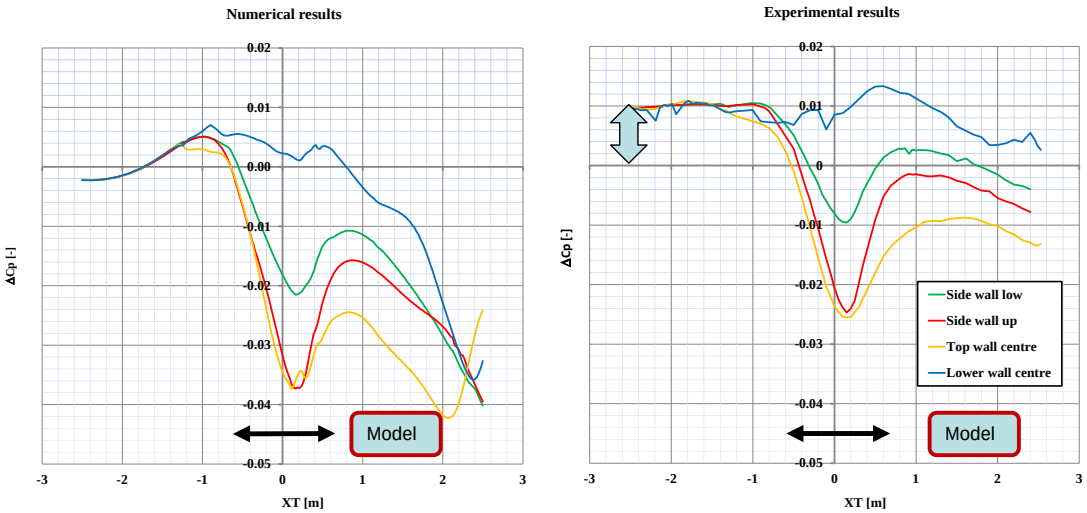

Figure 5-6: Tared wall pressure distributions from CFD (left) and experiment (right)

From table 5-2 it is concluded that the difference between de direct wall interference increment (Set A) and the numerical WIN3VE increment (set B based on CFD data) is 0.0015 in lift and 0.0002 in drag.

WIN3VE provides also corrections for blockage (ΔMa) and angle of attack ($\Delta\alpha$) as presented in table 5-2. These blockage and angle of attack corrections suggest that the test article experiences a different Mach number and angle of attack than the target values. For a proper comparison, additional computations are performed for the test article in free flow at the corrected Mach number (0.7837) and angle of attack (2.505°). If the corrections are sound, the increments in lift and drag between set A and B should decrease. Instead, the results show an increase in lift and drag differences between sets A and B which decided to stick to the standard approach to only correct for the wall-induced buoyancy effect.

5.4 Corrected results versus free flow results

Empty test section, support and wall interference corrections are applied to the test article in the numerical wind tunnel environment and compared to the free flow drag and lift results, see figure 5-7 and 5-8 respectively. Figure 5-7 shows that support and wall interference partly compensate and that the corrected drag coefficient deviates by 0.0002 from the free flow data. For the lift coefficient, a difference of 0.007 is obtained between the corrected wind tunnel results and the free flow data. The increment would have been 0.0015 in case the support interference increment of set 1 of table 5-1 is used in the correction procedure. For the drag coefficient, the difference would have been 0.0004 in case the increment of set 1 is used for the support effects. The presented differences are in the order of the experimental uncertainty which is ±0.003 for lift and ±0.0002 for drag.

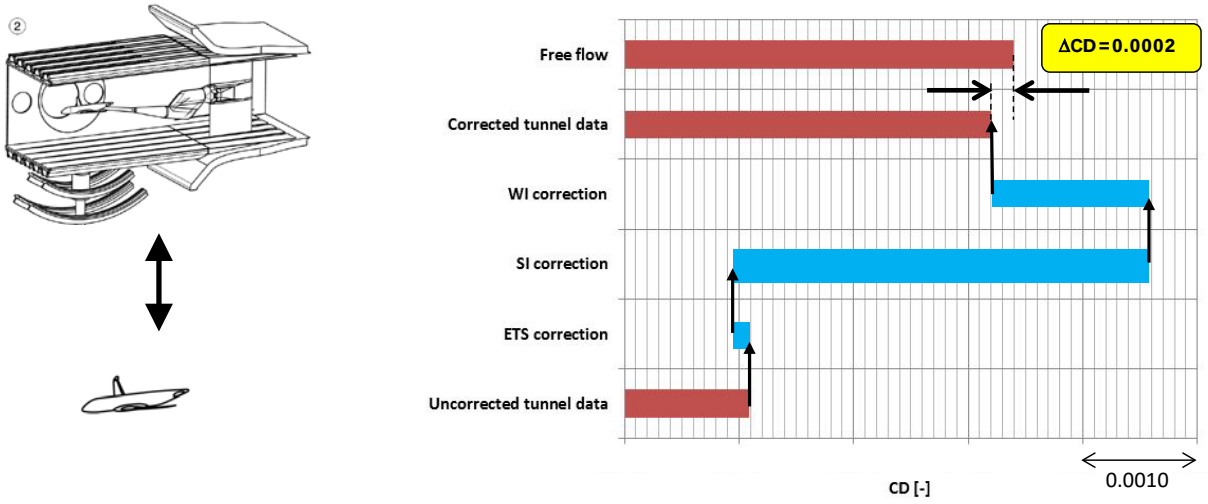

Figure 5-7: Correction steps based on CFD simulations of wind tunnel for drag results in comparison to free flow results; Ma=0.78 and alpha=2.5°

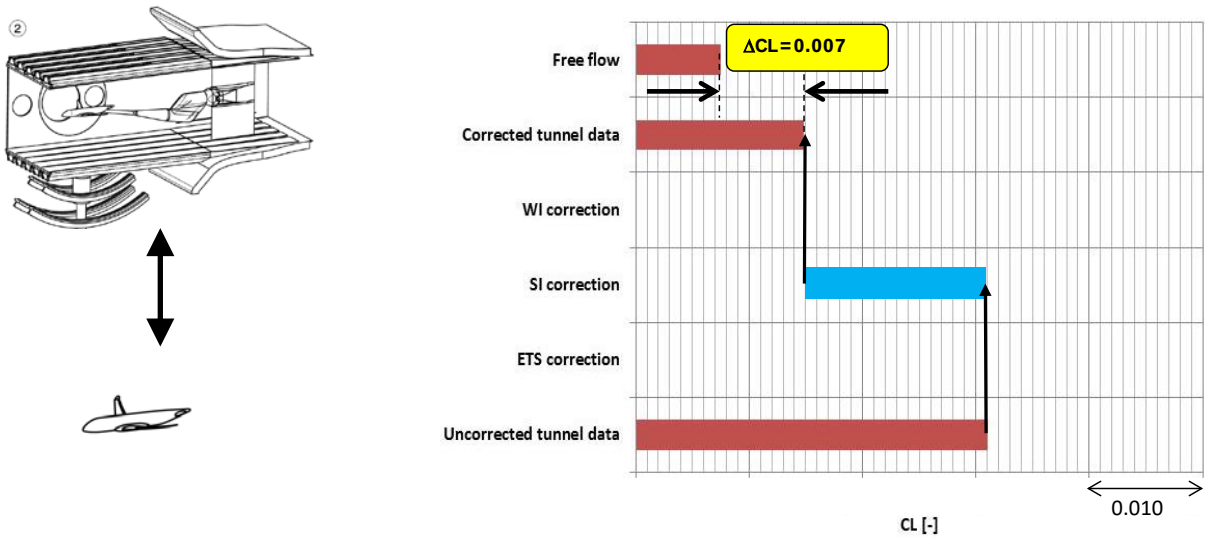

Figure 5-8: Correction steps based on CFD simulations of wind tunnel for lift results in comparison to free flow results; Ma=0.78 and alpha=2.5°

6.0 Conclusions

To verify the wind tunnel interference correction bookkeeping at DNW-HST, CFD has been utilized to generate aerodynamic performance data for a full-span test article around cruise condition. Numerical simulations are made for the test article in a wind tunnel environment (including the model support system and the slotted test section walls), as well as in free flow condition. Further, numerical simulations are conducted to establish the interference of the empty test section, the model support system and the wall-test article interactions. These attributions are consequently used to correct the 'in wind tunnel environment' CFD results in the same way the experimental data is commonly corrected at DNW-HST. After correction, the residuals of the computed drag and lift coefficients are 0.0002 and 0.007 with respect to free flow results.

These residuals are in the order of the achievable uncertainty levels in experiment and are therefore interpreted as a confirmation that the correction bookkeeping is adequate for achieving unbounded flow results from a slotted-wall wind tunnel alike DNW-HST.

References

[1] Wubben, F., and Takara, E., "Wind tunnel model support and wall interference corrections in DNW-HST – ensuring high data quality standards", *5th CEAS air & Space conference*, 7-11 September 2015 Delft, The Netherlands.

[2] Gebbink, R., Kapteijn, C., Bai, F., Mao, K., Zhang, D., Ba, Y., Zhang, M., "Consistency verifications of the DNW-HST tunnel interference correction bookkeeping", AIAA-2018-2116, *2018 AIAA Aerospace Sciences Meeting*, AIAA SciTech Forum, Kissimmee, Florida.

[3] Elsenaar, A., and Han, S.O.T.H., "A Break-Down of Sting Interference Effects," NLR TP-91220 U, *Model Support Corrections in Wind Tunnels Symposium*, 16-17 May 1991, Marknesse, The Netherlands.

[4] Labrujère, Th. E.; Maarsingh, R. A.; Smith, J.; "Evaluation of Measured-Boundary-Condition methods for 3D subsonic wall interference", NLR Technical report TR 88072 U, 1988

[5] Kok, J.C., Spekreijse, S.P., Efficient and accurate implementation of the k-omega turbulence model in the NLR multi-block Navier-Stokes system, NLR Technical paper TP-2000-144 , 2000

[6] Dol, H.S., Kok, J.C., Oskam, B., Turbulence modelling for leading edge vortex flows, AIAA 2002-0843, 40th Aerospace Sciences Meeting & Exhibit, 14-17 January 2002, Reno, Nevada